ACS ENGINEERING Au
AN OPEN ACCESS JOURNAL OF THE AMERICAN CHEMICAL SOCIETY

pubs.acs.org/engineeringau
Article

Comprehensive Compilation on Esterification Reactions and Predicting Reaction Kinetics and Equilibrium Using PC-SAFT

Iman Bahrabadi Jovein, Sindi Baco, Gabriele Sadowski, Ferruccio Doghieri, Marco Giacinti Baschetti, Gangqiang Yu, Sébastien Leveneur, Julien Legros, and Christoph Held*

Cite This: ACS Eng. Au 2025, 5, 234−246
Read Online

ABSTRACT: Knowledge of the equilibrium and kinetics of reactions is critical for optimizing industrial chemical processes. In this study, the equilibrium and kinetics of esterification reactions were systematically investigated for a series of carboxylic acids (acetic acid, propionic acid, formic acid, and levulinic acid) and alcohols (methanol, ethanol, *n*-propanol, and *n*-butanol), giving a total set of 16 esterification reactions at different temperatures. First, formation properties of reactants and products were utilized to calculate the reaction equilibrium constants K_{eq} of these reactions. These were compared with K_{eq} values obtained by one equilibrium experiment coupled to PC-SAFT predictions. The comparison yielded outstanding agreement between PC-SAFT-assisted K_{eq} values and the formation-property-derived K_{eq} values. The K_{eq} values were then used in activity-based kinetic expressions, and the predicted reaction kinetics were validated against experimental data to demonstrate the model's accuracy. The deviations between PC-SAFT and experimental data were AAD% (K_{eq}) = 1.66% for the reaction equilibrium and AAD% (r) = 13.8% for the kinetic curves. The Arrhenius equation and van 't Hoff equation were applied to depict the temperature dependence of reaction rate constants and of K_{eq} for each esterification reaction in a range of 303.15−423.15 K. Thus, activity-based thermodynamic standard properties are provided in this work, guiding the optimization of esterification reactions in a broad range of conditions.

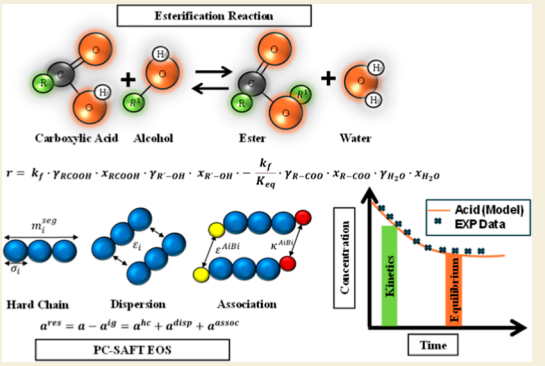

KEYWORDS: *thermodynamics, activity-based model, n-alcohols, carboxylic acids, Gibbs free energy of formation*

1. INTRODUCTION

Renewable and sustainable biomass has emerged as a promising energy source and is increasingly considered a practical substitute for fossil fuels. Made up of plant matter and organic residues, biomass presents a widely available and eco-friendly base for producing biofuels and biobased chemicals. By leveraging biomass in biofuel production, there is potential to lower greenhouse gas emissions and to decrease reliance on finite resources of our planet earth, supporting global initiatives aimed at addressing climate challenges.[1−4] Esterification is one of the important pathways in transforming biomass-derived materials into higher-value chemicals. This fundamental reaction yields ester synthesis from carboxylic acids with alcohols, and water is the only byproduct. Esterification plays a crucial role in biodiesel production, which involves renewable sources, such as vegetable oils, animal fats, and recycled waste oils. This process broadens the application potential of biomass-based feedstocks and enables the development of biolubricants, eco-compatible solvents, and a range of industrially essential compounds.[5] Notably, the use of short-chain alcohols such as methanol or ethanol has received attention in biodiesel production due to their advantageous reaction rates, availability, and cost-effectiveness.[6]

To optimize esterification reactions and their associated industrial processes, it is essential to understand the thermodynamics and kinetics of the reaction. These factors are influenced by the selected substrates and process conditions such as temperature, catalyst type, and liquid phase composition. Traditionally, experimental data are measured to capture the effects of the chosen substrate and all of the process conditions on the thermodynamics and kinetics of the esterification reactions. This is extremely time-consuming and resource-intensive. In contrast, predictive models offer a more efficient alternative by simulating molecular interactions and associated reaction behavior. Accurate determination of the equilibrium constant (K_{eq}) is crucial for predicting maximum reaction yields under various conditions. K_{eq} is important since it determines whether thermodynamic barriers are expected in the reaction limiting

Received: January 8, 2025
Revised: March 6, 2025
Accepted: March 7, 2025
Published: April 2, 2025

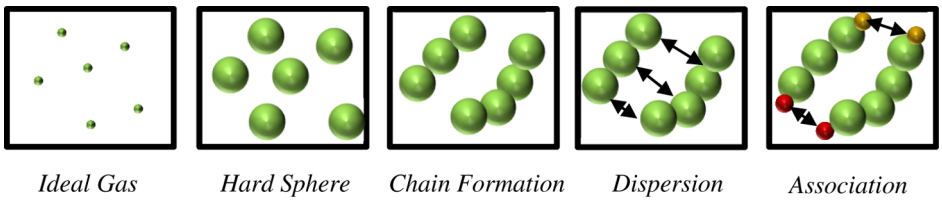

Figure 1. Schematic representation of the molecular model and the intermolecular interactions of the different contributions to the Helmholtz energy modeled with the PC-SAFT EOS.

the product yield. The yield can vary with factors such as reaction temperature, molar ratios of the reactants, and the specific solvent employed. Additionally, understanding the kinetics of these reactions must be known to offer insights into optimizing reaction rates in order to improve process efficiency.[7] This calls for the need for developing accurate predictive models for yield and kinetics in order to effectively design and scale-up esterification processes, ensuring enhanced efficiency and economic viability in industrial applications.

In contrast to several thermodynamic models such as UNIFAC or NRTL, perturbation-theory-based equations of state offer the advantage of having a higher accuracy for multicomponent mixtures.[8] Among these models, Perturbed-Chain Statistical Associating Theory (PC-SAFT), initially developed for complex systems involving association and dispersion, has demonstrated potential in accurately predicting phase behavior, kinetics, and equilibrium states in esterification reactions.[9] Nevertheless, various other models have been used to predict thermodynamics of esterification reactions, including g^E-models such as UNIFAC,[10] UNIQUAC,[11] and NRTL.[12] The big advantages of PC-SAFT in such mixtures of associating components have been demonstrated in the literature. Emel'yanenko et al.[13] investigated the esterification reaction between levulinic acid and three different alcohols with PC-SAFT and quantum-chemical calculations. Ascani et al.[14] used PC-SAFT for investigating phase equilibria in a reactive esterification system. Riechert et al.[15] studied the impact of solvents on esterification reactions involving acetic and propionic acids with ethanol. Their findings showed that acetonitrile was beneficial for acetic acid (AA) esterification. Using PC-SAFT, they successfully modeled the influence of solvents and solvent mixtures on equilibrium concentrations, aligning closely with the experimental data. Lemberg and Sadowski[9] conducted a study to predict the effects of various solvents, including acetonitrile, tetrahydrofuran, and dimethylformamide, on the reaction kinetics of esterification involving AA and propionic acid with ethanol. The PC-SAFT model was employed to predict the reaction kinetics and identify the optimal solvent for this case study under isothermal conditions with no change in the catalyst. Baco et al.[16] explored how the choice of solvent affects the reaction rate in the esterification of levulinic acid with ethanol, using sulfuric acid as a catalyst. They employed ePC-SAFT to estimate dissociation constants across various solvents, allowing them to separate the proton concentration from rate constants for more precise modeling. Their study found that solvents with low polarizability and strong hydrogen-bond acceptance led to faster reactions, with ethanol outperforming other investigated cosolvents, providing useful guidelines for selecting solvents in biomass conversion processes. Klinksiek et al.[2] utilized the advanced ePC-SAFT model to examine the impact of solvents and catalysts on the esterification of levulinic acid with ethanol, particularly under varying temperatures and catalyst concentrations. By predicting the reactant and catalyst activities and linking reaction kinetics to proton activity, catalyst effects without additional experimental data fitting could be predicted qualitatively correctly.

The present work aims to apply all of this gained knowledge for a broad scope of substrates in esterification reactions, including varying substrates and process conditions, with a focus on temperature. We aim at giving a comprehensive overview and a consistent thermodynamic data set on the equilibrium and kinetics by evaluating the accuracy of PC-SAFT-predicted equilibrium constants K_{eq} and reaction kinetics for a total of 16 esterification reactions in a temperature range of 303.15−423.15 K. K_{eq} was calculated and benchmarked against values derived from thermodynamic relationships utilizing the Gibbs free energy of formation. To incorporate the temperature dependency of Gibbs free energy, van't Hoff's relation was applied, enabling a robust and systematic evaluation across a range of thermal conditions.[17] This approach ensures a detailed and reliable prediction of the reaction behavior under variable temperatures. This work not only provides consistent data but also serves as an example to highlight the strengths of thermodynamic modeling for future applications in chemical engineering, particularly in systems where experimental data are scarce or difficult to obtain.

2. METHODS

2.1. PC-SAFT Equation of State: Theory and Parameters

In 2001, Gross and Sadowski[18] introduced a SAFT-based equation of state that treats the base fluid as a composition of hard chains. This adaptation of SAFT, known as PC-SAFT, builds on Wertheim's first-order perturbation theory alongside Barker and Henderson's second-order perturbation theory.[19] Initially, this equation was applied only to nonassociative fluids, but it was later expanded to account for additional effects, including terms for association forces.[20] Since then, parameters for PC-SAFT have been optimized for many pure components by using experimental data on vapor pressure and liquid density. As a result, PC-SAFT provides improved accuracy compared to the original SAFT model for both pure substances and binary mixtures.[21] A schematic representation of the PC-SAFT model is depicted in Figure 1. More details on PC-SAFT and the theory behind it can be found in Section S6 in the Supporting Information document.

The drawback of many other models is that they do not have the possibility to explicitly describe association-based intermolecular forces. In contrast, according to PC-SAFT, also such association forces are considered explicitly.[22] This yields finally an expression for the residual Helmholtz energy a^{res} based on Helmholtz energy contributions a^{hc}, a^{disp}, and a^{assoc}, which characterize forces induced by hard-chain repulsion, dispersive van der Waals attraction, and hydrogen bonding. This is illustrated in Figure 2 and expressed as

$$a^{res} = a - a^{ig} = a^{hc} + a^{disp} + a^{assoc} \quad (1)$$

Apart from the three parameters essential for characterizing simple fluids in their pure form, two additional parameters are required to explain associating interactions within a pure component.[23] These

https://doi.org/10.1021/acsengineeringau.5c00002
ACS Eng. Au 2025, 5, 234−246

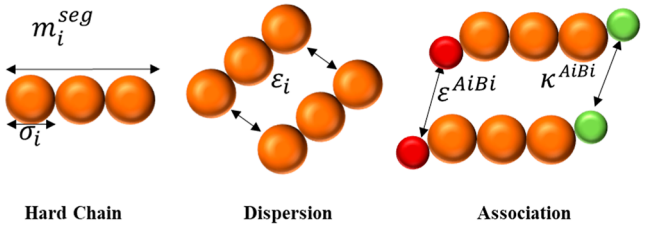

Figure 2. Schematic representation of the different parameters in the PC-SAFT EOS with association contribution, where the pure-component parameters are m_i^{seg}: segment number, σ_i: segment diameter, ε/k: dispersion−energy parameter, $\varepsilon^{A_iB_i}/k$: association−energy parameter, and $k^{A_iB_i}$: association−volume parameter.

parameters involve the association site pairs A_i and B_i: association−energy parameter ($\varepsilon^{A_iB_i}/k$) and association−volume parameter ($k^{A_iB_i}$).These parameters can be adjusted based on data specific to pure components. One can employ combining rules to measure the strength of cross-associating interactions between two substances with associating properties, as Wolbach and Sandler proposed.[24]

$$\varepsilon^{A_iB_j} = \frac{(\varepsilon^{A_iB_i} + \varepsilon^{A_jB_j})}{2} \tag{2}$$

$$k^{A_iB_j} = \sqrt{k^{A_iB_i}k^{A_jB_j}} \times \left(\frac{\sqrt{\sigma_{ii}\sigma_{jj}}}{1/2(\sigma_{ii} + \sigma_{jj})}\right)^3 \tag{3}$$

Further, appropriate combining rules are required that can be used to determine the parameters of the mixtures based on the parameters of the pure components.[25]

$$\varepsilon_{ij} = \sqrt{\varepsilon_{ii}\varepsilon_{jj}}(1 - k_{ij}) \quad k_{ij} \text{ is binary interaction parameter} \tag{4}$$

$$\sigma_{ij} = \frac{\sigma_{ii} + \sigma_{jj}}{2} \tag{5}$$

$$m = \sum_i x_i m_i \tag{6}$$

In this study, carboxylic acids, alcohols, and water are considered self-associating components, all with the 2B association scheme, while esters can only cross-associate, described by the induced-association approach. Induced association specifically examines mixtures in which at least one component does not self-associate but can form hydrogen bonds with other substances, such as water and alcohol. Building on the associating component mixing rules developed by Wolbach and Sandler, Kleiner and Sadowski introduced a straightforward method to account for this type of cross-association (termed "induced association") using only pure-component parameters.[26] Consequently, the cross-association parameters cannot be directly obtained using the standard combining rules.[26] This approach is based on the following assumptions[26]

- The association−energy parameter $\varepsilon^{A_iB_j}$ for the nonself-associating component is assigned to a value of zero.
- The association−volume parameter $k^{A_iB_j}$ for this component is assumed to match the corresponding parameter of the associating component within the mixture.

The more detailed introduction and equations for PC-SAFT EOS and induced association theory can be found in previous works[18,26].

2.2. PC-SAFT Pure-Component Parameters and Binary Interaction Parameters

The pure-component PC-SAFT parameters for most of the components analyzed in this study were sourced from existing literature and are detailed in Table 1.

In addition, the binary interaction parameters of PC-SAFT for different binary systems in considered esterification reactions are presented in Table 2. These are independent of the temperature for most of the mixtures.

2.3. Theory: Thermodynamic Fundamentals of Reaction

2.3.1. Standard Gibbs Free Energy Formation and Related Equilibrium Constant K_{eq}. The equilibrium constant applied in this work uses the standard state "pure component", where all

Table 1. PC-SAFT Pure-Component Parameters Esterification Reaction Participants

parameter	H_2O[2]	MeOH[2]	EtOH[2]	*n*-PrOH[26]	*n*-BuOH[2]	acetic acid[9]	methyl acetate[27]	ethyl acetate[9]	propyl acetate[27]
M [g·mol^{-1}]	18.015	32.042	46.07	60.096	74.12	60.052	74.079	88.11	102.13
m_i^{seg}[−]	1.2047	1.5255	2.3827	2.999	2.7515	1.3403	3.3301	3.5375	3.961
σ_i [Å]	2.7927	3.2300	3.1771	3.2522	3.6139	3.8582	3.1333	3.3079	3.3799
ε_i/k_B [K]	353.94	188.9	198.236	233.3967	259.5909	211.59	228.153	230.80	229.724
$\kappa^{A_iB_i}$ [−]	0.045099	0.0352	0.0324	0.015268	0.0067	0.07555	none	none	none
$\varepsilon^{A_iB_i}/k_B$ [K]	2425.7	2899.5	2653.38	2276.778	2544.56	3044.4	none	none	none
assoc scheme	2B	2B	2B	2B	2B	2B	none	none	none

	butyl acetate[27]	propionic acid[28]	methyl propanoate[27]	ethyl propanoate[9]	propyl propanoate[27]	butyl propanoate[27]	formic acid[29]	methyl formate[30]	ethyl formate[30]
M [g·mol^{-1}]	116.1583	74.079	88.106	102.13	116.159	130.1864	46.025	60.0524	74.0792
m_i^{seg} [−]	4.2911	3.7069	3.5358	3.8371	4.3772	4.5567	1.2956	2.678	2.888
σ_i [Å]	3.4476	2.9937	3.291	3.4031	3.4173	3.5264	3.3396	3.088	3.311
ε_i/k_B [K]	234.96	200.73	232.776	232.78	228.543	235.143	186.94	242.63	246.47
$\kappa^{A_iB_i}$ [−]	none	0.3205	none	0.045	none	none	0.2983	none	none
$\varepsilon^{A_iB_i}/k_B$ [K]	none	2173.4	none	none	none	none	2670.5	none	none
assoc scheme	none	2B	none		none	none	2B	none	none

	propyl formate[30]	butyl formate[31]	levulinic acid[13]	methyl levulinate[13]	ethyl levulinate[13]	propyl levulinate[32]	butyl levulinate[13]
M [g·mol^{-1}]	88.106	102.13	116.115	130.143	144.1684	144.1684	172.2215
m_i^{seg} [−]	3.209	3.591	2.0311	4.3566	6.4558	5.214	5.3007
σ_i [Å]	3.417	3.475	4.1241	3.4042	3.0938	3.4691	3.5910
ε_i/k_B [K]	246.46	246.1	266.49	277.09	226.93	263.07	265.15
$\kappa^{A_iB_i}$ [−]	none	none	0.0171	0.0351	0.0323	0.0152	0.00669
$\varepsilon^{A_iB_i}/k_B$ [K]	none	none	4578.36	none	none	none	none
assoc scheme	none	none	2B				

https://doi.org/10.1021/acsengineeringau.5c00002
ACS Eng. Au 2025, 5, 234−246

Table 2. Binary PC-SAFT Parameters k_{ij} Applied in This Work

no	binary system	binary interaction parameters (k_{ij})	reference
1	acetic acid and MeOH	0	
2	acetic acid and methyl acetate	0	
3	acetic acid and water	−0.13	15
4	MeOH and methyl acetate	0	
5	MeOH and water	−0.065	33
6	methyl acetate and water	−0.0147	34
7	acetic acid and EtOH	−0.03	15
8	acetic acid and ethyl acetate	−0.15	35
9	EtOH and ethyl acetate	−0.02	15
10	EtOH and water	−0.0382	2
11	ethyl acetate and water	−0.047	36
12	acetic acid and *n*-PrOH	0	
13	acetic acid and *n*-propyl acetate	0	
14	*n*-PrOH and *n*-propyl acetate	−0.012	37
15	*n*-PrOH and water	−0.017	38
16	*n*-propyl acetate and water	0	
17	acetic acid and *n*-BuOH	0.12	34
18	acetic acid and *n*-butyl acetate	−0.136	34
19	*n*-BuOH and *n*-butyl acetate	−0.011	37
20	*n*-BuOH and water	$2.94 \times 10^{-4} \times$T/K−0.102	39
21	*n*-butyl acetate and water	$4.50 \times 10^{-4} \times$T/K−0.161	40
22	propionic acid and MeOH	0.08	34
23	propionic acid and methyl propionate	0	
24	propionic acid and water	−0.0038	34
25	MeOH and methyl propionate	0	
26	methyl propionate and water	0	
27	propionic acid and EtOH	0	
28	propionic acid and ethyl propionate	−0.0354	34
29	ethanol and ethyl propionate	−0.008	37
30	ethyl propionate and water	$-0.0219 + 0.0003 \times (T/K - 298.15\ K)$	41
31	propionic acid and *n*-PrOH	0	
32	propionic acid and *n*-propyl propionate	0	
33	*n*-PrOH and *n*-propyl propionate	−0.012	37
34	*n*-propyl propionate and water	0	
35	propionic acid and *n*-BuOH	0	
36	propionic acid and *n*-butyl propionate	0	
37	*n*-BuOH and *n*-butyl propionate	0	
38	*n*-butyl propionate and water	0	
39	formic acid and MeOH	−0.2	34
40	formic acid and methyl formate	0	
41	formic acid and water	$-0.069 + 0.001062 \times (T/K - 298.15\ K)$	42
42	MeOH and methyl formate	−0.069	34
43	methyl formate and water	0	
44	formic acid and EtOH	0	
45	formic acid and ethyl formate	0	
46	EtOH and ethyl formate	0	
47	ethyl formate and water	0	
48	formic acid and *n*-PrOH	0	
49	formic acid and *n*-propyl formate	0	
50	*n*-PrOH and *n*-propyl formate	−0.0072	34
51	*n*-propyl formate and water	0	
52	formic acid and *n*-BuOH	0	
53	formic acid and *n*-butyl formate	0	
54	*n*-BuOH and *n*-butyl formate	0	
55	*n*-butyl formate and water	0	
56	levulinic acid and MeOH	−0.05	13
57	levulinic acid and methyl levulinate	0	
58	levulinic acid and water	−0.065	13,43
59	MeOH and methyl levulinate	$-0.0025\ T + 0.825$	43
60	Methyl levulinate and water	0	
61	levulinic acid and EtOH	0.03	13

https://doi.org/10.1021/acsengineeringau.5c00002
ACS Eng. Au 2025, 5, 234−246

Table 2. continued

no	binary system	binary interaction parameters (k_{ij})	reference
62	levulinic acid and ethyl levulinate	0.05	2
63	EtOH and ethyl levulinate	−0.02	2
64	ethyl levulinate and water	−0.06	2
65	levulinic acid and 1-PrOH	0	
66	levulinic acid and *n*-propyl levulinate	0	
67	*n*-PrOH and *n*-propyl levulinate	0	
68	*n*-propyl levulinate and water	0	
69	levulinic acid and 1-BuOH	0.02	13
70	levulinic acid and *n*-butyl levulinate	0	
71	*n*-BuOH and *n*-butyl levulinate	−0.00061 T + 0.1795	13
72	*n*-butyl levulinate and water	0.07	13,43

components are in their pure-component state, denoted as K_{eq}. It is expressed through the following eq 7, where $\Delta^R g^\circ$ represents the molar standard Gibbs free energy of the reaction, and R is the universal gas constant.[44]

$$K^\circ = \exp\left(\frac{-\Delta^R g^\circ}{RT^\circ}\right) \tag{7}$$

If T° refers to the tabulated temperature 298.15 K, then $\Delta^R g^\circ$ is also at 298.15. $\Delta^R g^\circ$ is described in terms of the respective enthalpy ($\Delta^R h^\circ$) and entropy ($\Delta^R s^\circ$) cf. Equation 8. Further, K_{eq} can be expressed through the following eq 9.[44]

$$\Delta^R g^\circ = \Delta^R h^\circ - T^\circ \Delta^R s^\circ \tag{8}$$

$$\ln K_{eq} = -\frac{\Delta^R h^\circ}{RT^\circ} + \frac{\Delta^R s^\circ}{R} \tag{9}$$

In this context, enthalpy and entropy of reaction in the standard state are defined as[44]

$$\Delta^R h^\circ = \left(\sum_i^N \Delta^f h^\circ\right)_{\text{products}} - \left(\sum_i^N \Delta^f h^\circ\right)_{\text{reactants}} \tag{10}$$

$$\Delta^R s^\circ = \left(\sum_i^N s^\circ\right)_{\text{products}} - \left(\sum_i^N s^\circ\right)_{\text{reactants}} \tag{11}$$

In eqs 10 and 11, $\Delta^f h^\circ$ refers to the molar standard enthalpy of formation, s° is the molar standard absolute entropy, and N represents the total number of all i products or reactants involved in the reaction. However, it is important to note that values for $\Delta^f h^\circ$ and s° are lacking for some components in the literature.[44]

The equilibrium constant at a specific temperature K_1 can be correlated using the integrated van 't Hoff equation using the known value of K°, under the assumption that the reaction enthalpy remains constant with temperature, cf. eq 12.

$$\frac{K_1}{K^\circ} = \frac{\Delta^R H^\circ}{R}\left(\frac{1}{T_1} - \frac{1}{T^\circ}\right) \tag{12}$$

Additionally, the enthalpy of formation of the liquid phase $\Delta^f h^{\circ,L}$ can be estimated by subtracting the enthalpy of vaporization Δh^{LV} from the enthalpy of formation of the gas phase $\Delta^f h^{\circ,V}$.[44]

$$\Delta^f h^{\circ,L} = \Delta^f h^{\circ,V} - \Delta h^{LV} \tag{13}$$

2.3.2. Reaction Kinetics and Equilibrium and Related Equilibrium Constant K_{eq}. In this study, the activity-based approach has been used to calculate the kinetics and equilibrium of reactions. The activity-based model incorporates the nonideal behavior of solutions, and it can be derived from a concentration-based model. For an equilibrium esterification reaction of carboxylic acids of the type RCOOH + R-OH ⇌ R-COO-R + H_2O, the reaction rate according to concentration-based (it assumes ideal mixture behavior) is[45]

$$r = k_f \cdot x_{\text{RCOOH}} \cdot x_{\text{R-OH}} - \frac{k_f}{K_{eq}} \cdot x_{\text{R-COO}} \cdot x_{H_2O} \tag{14}$$

where k_f represents forward reaction rate constants.

On the other hand, the reaction rate in terms of activity is

$$r = k_f \cdot \gamma_{\text{RCOOH}} \cdot x_{\text{RCOOH}} \cdot \gamma_{\text{R-OH}} \cdot x_{\text{R-OH}} - \frac{k_f}{K_{eq}} \cdot \gamma_{\text{R-COO}} \cdot x_{\text{R-COO}} \cdot \gamma_{H_2O} \cdot x_{H_2O} \tag{15}$$

To analyze the chemical equilibrium of reactions in the liquid phase based on the activity model, the mole fraction of component i (x_i) can be determined using eq 16. In this equation, the equilibrium constant is connected to the activities of the components within the reaction system. The activity of a component i reflects its effective concentration in relation to a chosen reference state.[2] For an esterification reaction, eq 17 can be used.

$$K_{eq}(T, P) = \exp\left(\frac{-\Delta^R g^0}{RT}\right) = \prod_i (x_i \gamma_i)^{\nu_i} = K_x K_\gamma \tag{16}$$

$$K_{eq} = \frac{a_{\text{ester}} a_{H_2O}}{a_{\text{acid}} a_{\text{alcohol}}} = \frac{x_{\text{ester}} x_{H_2O}}{x_{\text{acid}} x_{\text{alcohol}}} \times \frac{\gamma_{\text{ester}} \gamma_{H_2O}}{\gamma_{\text{acid}} \gamma_{\text{alcohol}}} \tag{17}$$

In this study, the PC-SAFT model is used for calculating the equilibrium constant according to the mole fractions of the reactants and products and their activity coefficients.

Also, the Arrhenius equation is a cornerstone of chemical kinetics, providing a quantitative relationship between the reaction rate constant and the temperature. This equation is defined as

$$\ln(k) = -\frac{E_a}{R} \cdot \frac{1}{T} + \ln(A) \tag{18}$$

where k represents the reaction rate constant, A is the pre-exponential factor, E_a is the activation energy, R is the universal gas constant, and T denotes the absolute temperature. The exponential dependence of the rate constant on temperature implies that even modest increases in temperature can lead to significant accelerations in the reaction rates, especially for reactions with high activation energies.

In this study, the effect of catalysts on reaction kinetics has been considered with an Arrhenius plot.

Furthermore, the equilibrium constant, K_{eq}, represents the ratio of the rate constants of the forward and reverse reactions at equilibrium. This relationship is expressed by eq 19.

$$K_{eq} = \frac{k_{\text{forward}}}{k_{\text{reverse}}} \tag{19}$$

3. CONSIDERED REACTIONS AND THERMODYNAMIC REACTION PROPERTIES

In this study, 16 esterification reactions were examined, and their equilibrium constants were calculated based on standard

https://doi.org/10.1021/acsengineeringau.5c00002
ACS Eng. Au 2025, 5, 234−246

Gibbs free energies of reactions. Subsequently, the thermodynamic properties of the components involved in each reaction, along with the calculations of the Gibbs free energy and equilibrium constants for each reaction, are presented.

In Table 3, the thermodynamic properties (standard enthalpy of formation, standard Gibbs free energy of formation, and standard entropy) of all of the reactants and products in the esterification reactions under study are listed.

Table 3. Molar Thermodynamics Properties in the Liquid Phase at $T°$ = 298.15 K, Standard Enthalpy of Formation ($\Delta^f h°$), Standard Gibbs Free Energy of Formation ($\Delta^f g°$), and Standard Entropy ($s°$)

n°	component	$\Delta^f h°$ [kJ/mol]	$\Delta^f g°$ [kJ/mol]	$s°$ [J/(mol K)]
1	water	−285.8[46]	−237.2[47]	69.9[44]
2	MeOH	−239.2[46]	−166.9[47]	126.8[46]
3	EtOH	−277.6[46]	−173.9[47]	160.7[46]
4	*n*-PrOH	−302.6[46]	−168.7[47]	193.6[46]
5	*n*-BuOH	−327.3[46]	−161.26[47]	225.8[46]
6	acetic acid	−484.3[46]	−389[47]	159.8[46]
7	methyl acetate	−445.9[46]	−328.39[48]	221.697[a]
8	ethyl acetate	−479.3[46]	−332.4[48]	262.339[a]
9	propyl acetate	−502.14[46]	−328.01[48]	305.2[a]
10	butyl acetate	−529.2[46]	−322.2[a]	334.95[48]
11	propionic acid	−510.7[46]	−381.59[47]	191.0[46]
12	methyl propionate	−464.75[46]	−320.76[a]	277.47[48]
13	ethyl propionate	−505.6[44]	−324.28[a]	291.5[44]
14	propyl propionate	−526.55[44]	−314.70[a]	323.3[44]
15	butyl propionate	−553.2[44]	−309.09[a]	355.1[48]
16	formic acid	−425.5[46]	−361.4[47]	131.84[46]
17	methyl formate	−386.1[44]	−297.4[49]	185.721[a]
18	ethyl formate	−421.85[44]	−305.59[a]	232.5[44]
19	propyl formate	−445.1[50]	−298.31[a]	264.3[44]
20	butyl formate	−437.1[48]	−283.413[a]	381.16[48]
21	levulinic acid	−685.25[46]	−401.664[a]	267.85[46]
22	methyl levulinate	−641.65[48]	−342.235[a]	351.15[48]
23	ethyl levulinate	−677.45[48]	−346.244[a]	383.74[48]
24	propyl levulinate	−703.18[48]	−341.62[a]	416.12[48]
25	butyl levulinate	−728.91[48]	−335.263[a]	448.5[48]

[a]Data was calculated by the thermodynamic relationship given in eq 8.

Table 4 presents all the reactions examined in this study, along with detailed calculations of the equilibrium constant $K_{eq}[\Delta^R g°(f)]$ for each reaction. These calculations are based on the data and thermodynamic properties listed in Table 3. Further, for these 16 reactions in Table 4, the $K_{eq}(T)$ has been calculated according to PC-SAFT using the activity-based approach shown in eq 17. This required one experimentally measured equilibrium concentration (at least) and all the corresponding activity coefficients of the reactants and products at the considered temperature. This information is given in detail in the Supporting Information section S1.

4. RESULTS AND DISCUSSION

4.1. Reaction Equilibrium

As a first result, the equilibrium constants were calculated using thermodynamic modeling using experimental equilibrium concentrations and activity coefficients predicted with PC-SAFT. These were compared with K_{eq} obtained from formation-properties-derived $\Delta^R g°$ values.

Figure 3 shows consistency between K_{eq} values (PC-SAFT vs formation-properties derived $\Delta^R g°$). This is a characteristic example that nicely shows the usefulness of both methods. That is, PC-SAFT is very suitable to model the properties of esterification mixtures quantitatively correctly. Further results for additional esterification reactions are available in Section S2 of the Supporting Information.

The absolute average deviation (AAD%) was calculated using eq 20. In this section, the AAD% was determined to evaluate the deviation between the equilibrium constants predicted by the PC-SAFT EOS activity-based model $[K_{eq}(\text{PC-SAFT})]$ and those calculated using the Gibbs free energy of formation $[K_{eq}(\text{formation})]$. The AAD% for these values was found to be 1.66%, indicating a high degree of agreement between the two methods

$$\text{AAD\%} = \frac{1}{N}\sum_{i=1}^{N}\left|\frac{K_{eq}(\text{formation}) - K_{eq}(\text{PC-SAFT})}{K_{eq}(\text{formation})}\right| \times 100 \quad (20)$$

To assess the accuracy of the PC-SAFT predictive model, we compared the equilibrium concentrations of AA (x_{eq}) obtained from the PC-SAFT prediction with those derived from experimental data for several reactions. This comparison serves as a validation of the predictive capability of PC-SAFT.

In Figure 4, the results show a high degree of consistency, highlighting the robustness of PC-SAFT in capturing the equilibrium behavior of different esterification reactions across various conditions.

We observed remarkable agreement between PC-SAFT and the experimental data in most of the considered systems (cf. Figures S1−S3). Nevertheless, in Figures 4 and S4 and S6, some deviations become obvious between PC-SAFT and the experimental data. One reason is that the experimental data were digitalized from graphical plots rather than numerical tables, so there are unavoidable uncertainties in data digitization. This may lead to small differences between the extracted equilibrium conversion and model predictions, as seen at 333.15 K in Figure 4. Further, experimental measurements have a non-negligible uncertainty. Also note that PC-SAFT results are predictions in the sense that no (not any) reaction data was used to fit any PC-SAFT parameters, which makes a small deviation unavoidable. The well-known and expected temperature-induced shift in equilibrium conversion for the esterification reactions cannot be observed in each experimental data set, e.g., experimental data[45] do not indicate any temperature effect on the equilibrium conversion while the formation-based data yield a nonzero enthalpy of the reaction. In summary, it should be emphasized that there is very good general agreement between experimental data and PC-SAFT prediction of the equilibrium mole fraction of the carboxylic acid, confirming the predictive capability and robustness of the proposed PC-SAFT-based approach.

Additional results for other esterification reactions are presented in Section S2 of the Supporting Information.

Furthermore, the absolute average deviation (AAD %) was calculated using eq 21 to assess the accuracy of the predicted equilibrium concentrations against the corresponding experimental data for various esterification reactions. The analysis resulted in an AAD % of 13.8%, indicating the degree of deviation between the predicted and the observed values.

https://doi.org/10.1021/acsengineeringau.5c00002
ACS Eng. Au 2025, 5, 234−246

Table 4. Calculations of Formation-Property Based (f) Reaction Properties and Resulting Equilibrium Constant $K_{eq}[\Delta^R g°(f)]$ at 298.15 K Obtained with eqs 9−11 Compared with Equilibrium Constant Obtained with eq 17 at Different Temperatures $[K_{eq}(T)]$

reaction no	esterification reaction	$\Delta^R h°(f)$ [kJ/mol]	$\Delta^R s°(f)$ [J/mol K]	$\Delta^R g°(f)$ [kJ/mol]	$K_{eq}(\Delta^R g°(f))$	$K_{eq}(T)$ eq 17	T [K]
1	acetic acid + MeOH ⇌ methyl acetate + water	−8.2	4.997	−9.69	49.855	38.597	323.15
						35.218	333.15
2	acetic acid + EtOH ⇌ ethyl acetate + water	−3.2	11.739	−6.7	14.922	14.608	303.15
						13.504	323.15
3	acetic acid + n-PrOH ⇌ propyl acetate + water	−1.04	21.7005	−7.51	20.690	19.582	343.15
						19.381	353.15
4	acetic acid + n-BuOH ⇌ butyl acetate + water	−3.4	19.25	−9.139	39.924	33.352	343.15
						32.245	353.15
5	propionic acid + MeOH ⇌ methyl propionate + water	−0.69	25.57	−9.466	45.552	44.984	313.15
						44.315	333.15
6	propionic acid + EtOH ⇌ ethyl propionate + water	−3.1	9.7	−5.992	11.215	10.367	318.15
						10.003	328.15
7	propionic acid + n-PrOH ⇌ propyl propionate + water	0.95	8.6	−1.614	1.917	1.943	308.15
						1.986	328.15
8	propionic acid + n-BuOH ⇌ butyl propionate + water	−1	8.2	−3.444	4.013	3.806	343.15
						3.769	353.15
9	formic acid + MeOH ⇌ methyl formate + water	−7.2	−3.018	−6.3	12.699	12.105	303.15
						10.143	323.15
10	formic acid + EtOH ⇌ ethyl formate + water	−4.55	9.86	−7.489	20.522	14.190	373.15
						11.932	423.15
11	formic acid + n-PrOH ⇌ propyl formate + water	−2.8	8.76	−5.411	8.874	7.652	343.15
						7.443	353.15
12	formic acid + n-BuOH ⇌ butyl formate + water	29.9	93.42	2.046	0.437	2.129	343.15
						2.865	353.15
13	levulinic acid + MeOH ⇌ methyl levulinate + water	−3	26.4	−10.871	80.288	78.701	303.15
						73.111	323.15
14	levulinic acid + EtOH ⇌ ethyl levulinate + water	−0.4	25.09	−7.880	24.026	23.728	323.15
						23.523	343.15
15	levulinic acid + n-PrOH ⇌ propyl levulinate + water	−1.13	24.57	−8.455	30.299	28.222	353.15
						28.540	343.15
16	levulinic acid + n-BuOH ⇌ butyl levulinate + water	−2.16	24.75	−9.539	46.912	43.854	323.15
						40.959	353.15

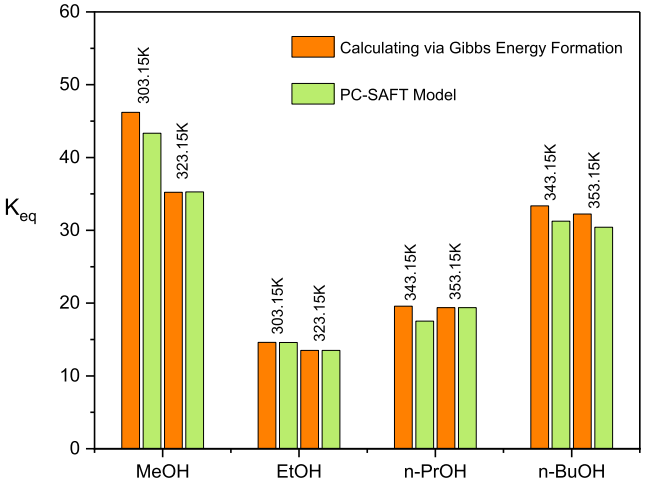

Figure 3. Reaction equilibrium constants K_{eq} according to Table 4 of AA esterification with different alcohols at p = 1 bar and different temperatures. Green: Predicted with PC-SAFT and the parameters given in Tables 1 and 2. Orange: Obtained from formation properties derived $\Delta^R g°$ values with formation properties from Table 3.

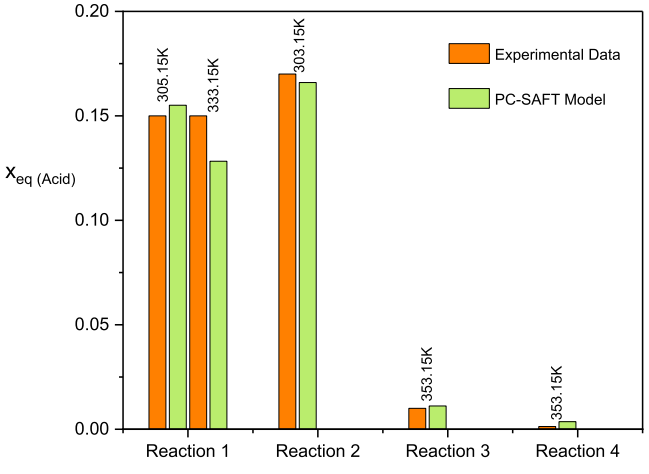

Figure 4. Comparing the equilibrium mole fraction of AA in different esterification reactions at p = 1 bar and at different temperatures. Reaction numbers according to Table 4. PC-SAFT prediction using the parameters given in Tables 1 and 2 (green) vs experimental data (orange) with literature data from reaction 1,[45] reaction 2,[9] and reaction 3,4.[51]

https://doi.org/10.1021/acsengineeringau.5c00002
ACS Eng. Au 2025, 5, 234−246

Table 5. Parameters of Reaction Kinetics for Considered Esterification Reactions

reaction no	esterification reaction	E_a [kJ/mol]	k [1s]	T [K]
1	acetic acid + MeOH ⇌ methyl acetate + water	44.355	0.00277	323.15
			0.00448	333.15
2	acetic acid + EtOH ⇌ ethyl acetate + water	35.658	0.00084	303.15
			0.00202	323.15
3	acetic acid + *n*-PrOH ⇌ propyl acetate + water	38.085	0.000065	323.15
			0.000217	353.15
4	acetic acid + *n*-BuOH ⇌ butyl acetate + water	37.147	0.000138	343.15
			0.0000617	323.15
5	propionic acid + MeOH ⇌ methyl propionate + water	26.025	0.000018	313.15
			0.00003280	333.15
6	propionic acid + EtOH ⇌ ethyl propionate + water	15.238	0.000163	318.15
			0.000194	328.15
7	propionic acid + *n*-PrOH ⇌ propyl propionate + water	31.923	0.000147	308.15
			0.00031	328.15
8	propionic acid + *n*-BuOH ⇌ butyl propionate + water	37.467	0.000031	323.15
			0.0001001	353.15
9	formic acid + MeOH ⇌ methyl formate + water	20.485	0.0127	303.15
			0.021	323.15
10	formic acid + EtOH ⇌ ethyl formate + water	20.300	0.00042	373.15
			0.00091	423.15
11	formic acid + *n*-PrOH ⇌ propyl formate + water	26.187	0.0000617	313.15
			0.000185	353.15
12	formic acid + *n*-BuOH ⇌ butyl formate + water	50.048	0.000081	323.15
			0.000242	343.15
13	levulinic acid + MeOH ⇌ methyl levulinate + water	16.310	0.00003	303.15
			0.0018	323.15
14	levulinic acid + EtOH ⇌ ethyl levulinate + water	67.563	0.000204	323.15
			0.00088	343.15
15	levulinic acid + *n*-PrOH ⇌ propyl levulinate + water	74.572	0.000014	303.15
			0.000090	323.15
16	levulinic acid + *n*-BuOH ⇌ butyl levulinate + water	46.026	0.00014	323.15
			0.0006	353.15

$$\mathrm{AAD\%} = \frac{1}{N}\sum_{i=1}^{N}\left|\frac{x_{i,eq}(\text{PC-SAFT}) - x_{i,eq}(\exp)}{x_{i,eq}(\exp)}\right| \times 100 \tag{21}$$

4.2. Reaction Kinetics

Kinetics plays a pivotal role in esterification reactions, influencing both the reaction rate and yield, which are critical parameters in industrial applications such as biodiesel production, pharmaceuticals, and food processing. Unlike reactions that reach equilibrium quickly, esterification is both kinetically and thermodynamically limited, meaning that understanding and accurately predicting its kinetics is essential for optimizing conditions to achieve desired yields within practical timeframes in order to allow high space-time yields. The rate of esterification reactions is particularly sensitive to both the catalyst presence and reaction conditions, notably temperature. Kinetic data are essential for determining optimal operating conditions that balance reaction speed with efficiency, as higher temperatures generally accelerate esterification reactions but may also introduce undesirable side reactions or energy costs. As such, reliable kinetic models are crucial to minimizing reaction time while maximizing yield, enabling more efficient process design and control in industrial applications. In this work, we do not consider side reactions and we do not focus on catalyst effects. Rather, we predict reactant activity under different conditions to then predict kinetic curves.

The present work does not account for side reactions in the kinetic model scheme. However, under practical conditions, side reactions such as transesterification and etherification can lead to small variations in reaction rates as well as in positions of equilibrium, as in several studies on esterification reaction, the side reactions have not been considered.[15,52,53]

Note, the research is largely centered on equilibrium modeling, whereby catalyst effects are not significant as catalysts change neither the end equilibrium position but rather the rate at which equilibrium is established. Thus, catalyst effects have not been considered in the present work; i.e., the catalytic influence of concentration on the rate constant is not taken into account. The research adopts a constant catalytic environment assumption, where the catalyst concentration is maintained constant throughout experiments, ruling out variability in catalytic effects.

The temperature dependence of the kinetics is properly represented in the description of the rate constant of the reaction. Catalysts, in the case here, the proton, operate predominantly as accelerator functions by protonation of the carboxylic acid functional group.

4.2.1. Activity-Based Kinetic Parameters: Activation Energy and Kinetic Constant. The activity-based model, coupled with the PC-SAFT EOS, was utilized in this study to predict the kinetics of the esterification reaction. In the kinetic

https://doi.org/10.1021/acsengineeringau.5c00002
ACS Eng. Au 2025, 5, 234−246

analysis, the activation energy and reaction rate constant are critical parameters. These parameters have been determined for all the reactions considered in this study, as summarized in Table 5.

4.2.2. Temperature Effect on Esterification Kinetics. Temperature is a key factor influencing the esterification kinetics. Higher temperatures typically increase reaction rates due to enhanced molecular motion and collision frequency, thus accelerating the formation of ester products. However, elevated temperatures shift equilibrium toward the reactant side of exothermic reactions, potentially limiting the maximum achievable yield of esterification under certain conditions. Additionally, high temperatures may lead to degradation of certain reactants or products, especially in sensitive applications, such as pharmaceuticals. Thus, understanding the kinetic response to temperature variations allows for the optimization of reaction conditions, helping to strike a balance between the reaction rate and product stability.

The temperature dependence of the reaction rate constants is described using the Arrhenius eq (eq 18). To illustrate this relationship, Arrhenius plots for all reactions are presented in Section S4 of the Supporting Information.

The fitting in Section S4 is based on the available experimental data, which, in some cases, consist of only a few equilibria points and only two experimental kinetic constants due to limitations in the referenced literature. Obviously, using only two experimental kinetic constants to derive the activation energy E_a that is required in the modeling is a critical step (two points are the minimum; three points are at least desired). However, PC-SAFT has been validated before using multiple data sets, and its predictive capability was benchmarked in the equilibrium sections before against formation-property-based equilibrium constants. The consistency between PC-SAFT predictions and formation-property-derived equilibrium constants has supported the reliability of the model, even when the number of available data points is limited. Thus, we might expect a robust model response even using only a minimal experimental data set used to adjust the PC-SAFT-based activation energy.

In Figure 5, the impact of temperature on the esterification reaction was evident, as increasing the reaction temperature led to a noticeable enhancement in the reaction rate constant at a fixed reactant mole ratio MR. The findings further revealed that elevated temperatures significantly reduced the time required for acid conversion, highlighting the essential role of temperature optimization in improving the reaction performance and efficiency. Additional kinetic results for other esterification reactions are presented in Section S3.1 of the Supporting Information.

4.2.3. Esterification of Different Acids with Methanol. In this study, we performed a comparison showcasing the esterification reactions between methanol (MeOH) and four different acids at a constant temperature. This comparison aims to provide a clear visual representation of how various carboxylic acids behave under identical reaction conditions, offering insights into the kinetics and equilibrium characteristics of each reaction.

Figure 6 presents the kinetic profiles of esterification reactions between methanol (MeOH) and four different acids: levulinic acid, AA, propionic acid, and formic acid, at a temperature of 323.15 K. The figure highlights the differences in reaction profiles, such as reaction rates and equilibrium conversions, when MeOH is esterified with different acids.

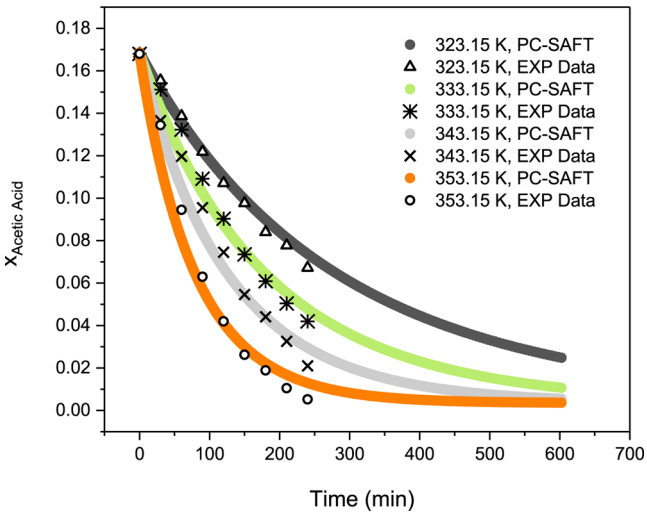

Figure 5. Mole fraction of AA during esterification with n-butanol at different temperatures and 1 bar. MR = 4 (1:4 mol ratio of acid/alcohol). Symbols: Experimental data taken from.[51] Lines: PC-SAFT prediction using parameters from Tables 1, 2, and 5.

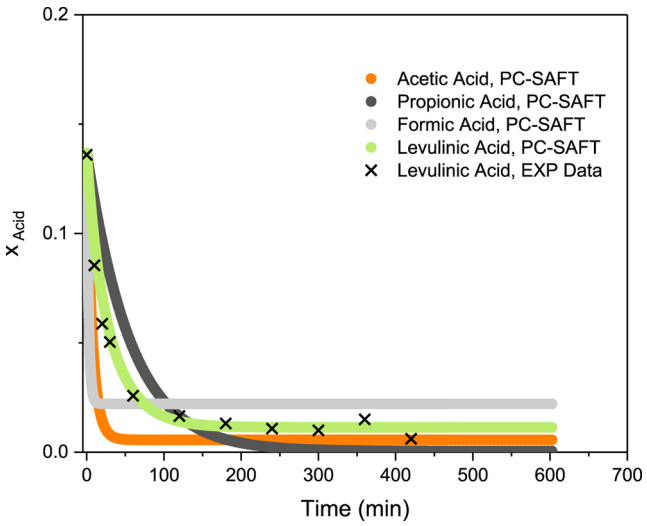

Figure 6. Kinetics of the esterification reaction of MeOH with different carboxylic acids at 323.15 K at 1 bar. For all acids: MR (mol ratio of acid/alcohol) = 1:6.5, symbols: experimental data from.[54] Lines: PC-SAFT prediction using parameters from Tables 1, 2, and 5.

These acids were chosen to represent a range of molecular structures and reactivity patterns, thereby allowing for a comprehensive analysis of how structural variations impact the esterification process. It can be observed that the kinetics of the formic acid + MeOH reaction is similar to the kinetics of the AA + MeOH reaction, but the equilibria are different.

Formic acid kinetics using MeOH yielded the fastest kinetics among the chosen reactant partners. This suggests that formic acid reacts more rapidly with methanol compared to the other acids, likely due to its smaller molecular structure and higher reactivity. The PC-SAFT model predictions for levulinic acid align reasonably well with the experimental data.

4.2.4. Esterification of AA with Different Alcohols. In this study, we include a comparison that illustrates the esterification reactions of a single acid with four different alcohols at a constant temperature. This comparison is essential for visualizing how the choice of alcohol influences

https://doi.org/10.1021/acsengineeringau.5c00002
ACS Eng. Au 2025, 5, 234−246

the reaction kinetics and equilibrium positions under identical experimental conditions, i.e., the same temperature and MR.

Figure 7a presents the kinetic profiles of AA esterification with four alcohols: MeOH, EtOH, *n*-PrOH, and *n*-BuOH at

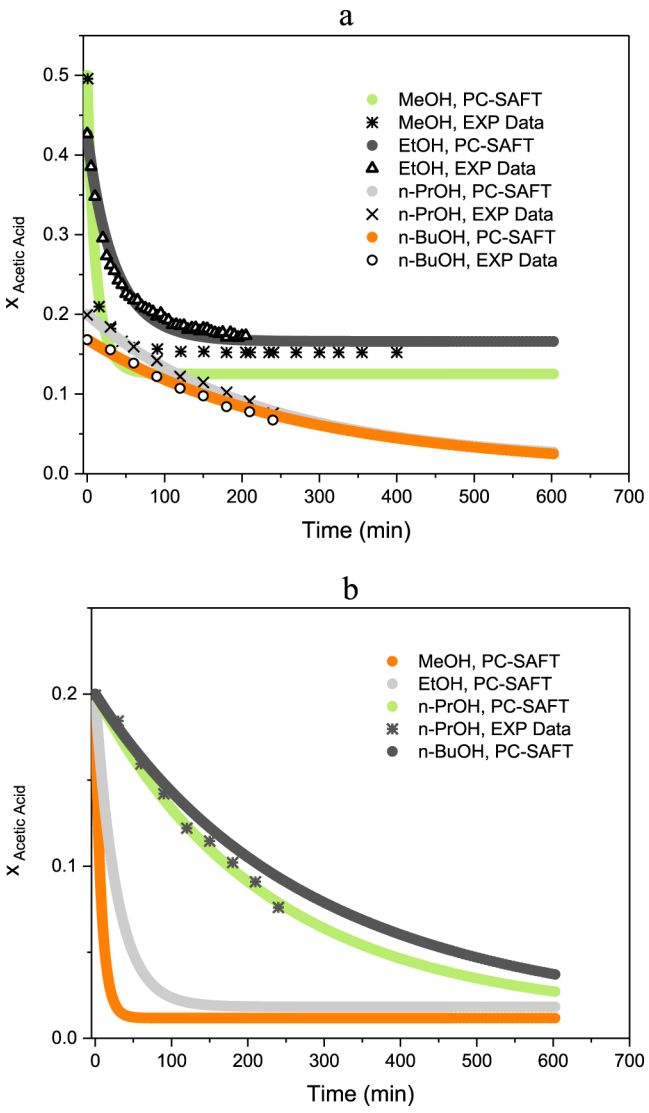

Figure 7. Mole fraction of AA during esterification with different alcohols at 323.15 K and 1 bar. (a) MeOH and EtOH: MR (acid/alcohol) = 1, *n*-PrOH: MR = 4, and *n*-BuOH: MR = 5. (b) MR (acid/alcohol) = 4 for all alcohols. Symbols: experimental data for MeOH,[45] EtOH,[9] and *n*-PrOH and *n*-BuOH.[51] Lines: PC-SAFT prediction using parameters from Tables 1, 2, and 5.

323.15 K and 1 bar. The analysis utilizes varying MRs of acid to alcohol: 1:1 for MeOH and EtOH, 1:4 for *n*-PrOH, and 1:5 for *n*-BuOH. The predictions of the PC-SAFT-assisted activity-based kinetic model are compared against experimental data, showcasing the ability to capture the effects of diverse alcohol types on kinetics and equilibria. The figure captures key metrics, such as reaction rate profiles, equilibrium conversions, and deviations between predicted and experimental outcomes. By comparing these reactions, the figure highlights the variability in esterification behavior when the acid interacts with alcohols of differing chain lengths, branching groups, or functional groups.

Figure 7b presents the kinetics of the esterification reactions of AA with various alcohols, including methanol (MeOH), ethanol (EtOH), *n*-propanol (*n*-PrOH), and *n*-butanol (*n*-BuOH), at a temperature of 323.15 K and under identical molar ratios (MR = 4). The figure provides a clear basis for comparison, revealing that the equilibrium conversion decreases as the size and complexity of the alcohol molecule increase. The observed trend follows the order: MeOH > EtOH > *n*-PrOH > *n*-BuOH.

The results reveal that methanol and ethanol exhibit significantly faster conversion rates compared with *n*-propanol and *n*-butanol. Methanol achieves the quickest reaction completion, likely due to its smaller molecular size and reduced steric hindrance, which facilitates higher reactivity. Conversely, *n*-butanol demonstrates the slowest conversion rate, which is attributed to its larger molecular size and greater steric effects. Ethanol and *n*-propanol exhibit intermediate conversion rates, underscoring the influence of the chain length and alcohol structure on the kinetics of the esterification process.

The PC-SAFT model closely replicates the experimental trends for all alcohols, reinforcing its predictive accuracy and utility for both thermodynamic and kinetic analyses. These findings emphasize the critical role of the alcohol type in influencing reaction rates, with shorter-chain alcohols (e.g., methanol and ethanol) enabling faster conversions and longer-chain alcohols requiring extended reaction times or tailored conditions. Note, it can be observed from Figure 7a that the equilibrium concentration of AA upon esterification with MeOH is underestimated with PC-SAFT, which might be caused by experimental uncertainty, digitalization uncertainties of the data, or PC-SAFT uncertainties in highly accurate modeling short-chain alcohol interactions with the reaction medium. Despite this slight underestimation for esterification with MeOH, the deviation remains within a reasonable range and does not significantly downgrade the overall success of the reaction equilibrium prediction; note again that not a single PC-SAFT parameter was adjusted to any reaction data.

Figure 8 highlights the versatility of the PC-SAFT model as a valuable tool for optimizing esterification reactions across various alcohol systems. Figure 8a illustrates the kinetic behavior of levulinic acid esterification with MeOH, EtOH, *n*-PrOH, and *n*-BuOH at 323.15 K and 1 bar. The acid-to-alcohol MRs vary by alcohol: 6.5 for MeOH, 4 for EtOH, and 4 for *n*-PrOH and *n*-BuOH. The predictions from the PC-SAFT model are compared to experimental data, demonstrating the model's effectiveness in describing reaction kinetics. Note that excess water was used in the original reference for the reactions with *n*-PrOH and *n*-BuOH. While it is well-known that excess water will negatively influence the kinetics and reaction equilibrium of any esterification reaction, it was used here as a model substance to stress PC-SAFT in its prediction performance to study the effect of water on kinetics and equilibria.

Figure 8b represents the kinetics of the esterification reaction of levulinic acid with different alcohols (methanol, ethanol, *n*-propanol, and *n*-butanol) at 323.15 K and under identical molar ratios (MR = 4). Figure 8b shows that the mole fraction of levulinic acid ($x_{\text{levulinicacid}}$) depends strongly on the type of alcohol.

Distinct reaction profiles are observed for each alcohol. Using methanol achieves the fastest reaction rate, completing the conversion of levulinic acid in a shorter time due to its high

https://doi.org/10.1021/acsengineeringau.5c00002
ACS Eng. Au 2025, 5, 234−246

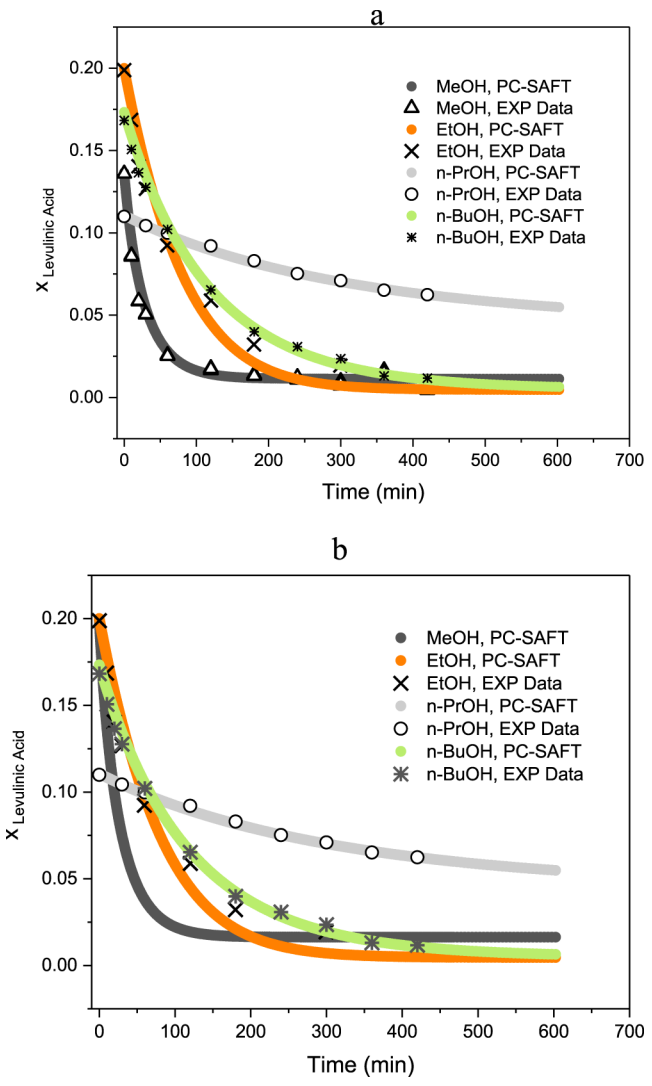

Figure 8. Mole fraction of levulinic acid during esterification with different alcohols at 323.15 K and 1 bar. (a) MeOH (acid/alcohol) = 6.5, EtOH: MR = 4, *n*-PrOH and *n*-BuOH (with water as a solvent) MR = 4. (b) MR (acid/alcohol) = 4 for all alcohols. Symbols: experimental data for MeOH, EtOH,[54] and *n*-PrOH and *n*-BuOH.[32] Lines: PC-SAFT prediction using parameters from Tables 1, 2, and 5.

reactivity and minimal steric hindrance. In contrast, *n*-butanol exhibits the slowest reaction rate, reflecting the influence of its larger molecular structure and steric effects. Ethanol and *n*-propanol display intermediate reaction rates, forming a progression from methanol to n-butanol, which highlights the impact of the alcohol chain length and molecular structure on reaction kinetics.

To sum up, by comparing experimental data with the modeling outcomes, it can be stated that thermodynamics theory can be benchmarked against real-world results. The comparison supports the accuracy of the model and identifies any discrepancies that warrant further investigation. These findings underscore the importance of selecting appropriate alcohols to optimize the reaction rates. The analysis reaffirms the PC-SAFT model as a robust tool for modeling esterification kinetics and designing efficient processes for applications such as biofuels and specialty chemicals. It is important to mention that catalyst effects are not considered in this work. In order to consider the effect of catalyst (H_2SO_4) on the esterification reaction, please refer to S5 of Supporting Information.

In the future, our results can be used to optimize real reactions in real reactor systems. For this, please note that we have not performed process simulation. The PC-SAFT predictions in this work can only be transferrable to a setup with an ideally mixed reactor (batch) operating at constant temperature and atmospheric pressure. No explicit consideration was given to mass transfer limitations, hydrodynamics, or external effects such as phase separation, as the focus was on the intrinsic reaction kinetics and equilibrium behavior. Additionally, no phase equilibria vapor−liquid was considered, and a transfer to a reactor setup must assume that there is no mass loss due to partial evaporation.

5. CONCLUSIONS

This study demonstrates that the PC-SAFT EOS activity-based model, combined with experimental data, provides a robust and consistent framework for analyzing the equilibrium and kinetics of esterification reactions. By accurately predicting equilibrium constants and using only one fitted activity-based kinetic constant per esterification reaction, the model effectively addresses both the thermodynamics and kinetics of these reactions. The predictions of equilibrium constants using PC-SAFT and Gibbs free energy of formation showed excellent accuracy, with an AAD % value of 1.66%, while the equilibrium concentrations compared to experimental data resulted in an AAD % of 13.8%. These results confirm that PC-SAFT predictions align closely with experimental observations, enabling the effective modeling of reaction behavior across diverse conditions.

The study underscores that the equilibrium constant (K_{eq}) can be derived based on formation properties if such data are available. If not, PC-SAFT allows for a proper prediction using only one experimental equilibrium concentration. The agreement between the experimental data and PC-SAFT predictions highlights the ability of PC-SAFT to reduce the experimental effort typically required for reaction optimization. Achieving a reliable description of esterification equilibrium and kinetics required precise predictions of reactant activities, accurate determination of K_{eq}, and the application of adjusted kinetic constants, thereby supporting a comprehensive framework for modeling esterification reactions. The application of the Arrhenius equation depicted the temperature dependence of reaction rate constants, while the influence of temperature on esterification performance was explored over the range of 303.15−423.15 K. Results demonstrated that higher temperatures significantly reduced acid conversion times, underscoring the critical role of temperature in optimizing reaction conditions.

Furthermore, the study analyzed the esterification behavior of individual acids with various alcohols and individual alcohols with different acids under constant temperature conditions, providing valuable insights into the impact of reactant combinations on the reaction dynamics. Overall, PC-SAFT proves to be a powerful tool for the efficient design and optimization of esterification processes with potential applications across industries such as pharmaceuticals, food, and biodiesel production. This approach enhances predictive accuracy and reduces the time and resources needed for experimental validation, paving the way for a more streamlined and cost-effective process development.

https://doi.org/10.1021/acsengineeringau.5c00002
ACS Eng. Au 2025, 5, 234−246

■ ASSOCIATED CONTENT

Supporting Information

The Supporting Information is available free of charge at https://pubs.acs.org/doi/10.1021/acsengineeringau.5c00002.

Calculation of the equilibrium constant of the 16 esterification reactions under study, together with the mole fractions at equilibrium; comparison of formation-property-based equilibrium constants with the PC-SAFT modeled equilibrium constant; comparison of PC-SAFT predicted equilibrium mole fractions with experimental data; comparison of PC-SAFT predicted kinetic curves until equilibrium with experimental data; Arrhenius plots; and PC-SAFT fundamentals (PDF)

■ AUTHOR INFORMATION

Corresponding Author

Christoph Held − *Laboratory of Thermodynamics, Department of Biochemical and Chemical Engineering, TU Dortmund University, Dortmund 44227, Germany;* orcid.org/0000-0003-1074-177X; Email: christoph.held@tu-dortmund.de

Authors

Iman Bahrabadi Jovein − *Department of Civil, Chemical, Environmental and Materials Engineering, University of Bologna, Bologna 40126, Italy; Laboratory of Thermodynamics, Department of Biochemical and Chemical Engineering, TU Dortmund University, Dortmund 44227, Germany*

Sindi Baco − *Laboratory of Thermodynamics, Department of Biochemical and Chemical Engineering, TU Dortmund University, Dortmund 44227, Germany*

Gabriele Sadowski − *Laboratory of Thermodynamics, Department of Biochemical and Chemical Engineering, TU Dortmund University, Dortmund 44227, Germany;* orcid.org/0000-0002-5038-9152

Ferruccio Doghieri − *Department of Civil, Chemical, Environmental and Materials Engineering, University of Bologna, Bologna 40126, Italy;* orcid.org/0000-0002-6140-2324

Marco Giacinti Baschetti − *Department of Civil, Chemical, Environmental and Materials Engineering, University of Bologna, Bologna 40126, Italy;* orcid.org/0000-0002-7327-1608

Gangqiang Yu − *Laboratory of Thermodynamics, Department of Biochemical and Chemical Engineering, TU Dortmund University, Dortmund 44227, Germany; College of Environmental Science and Engineering, Beijing University of Technology, Beijing 100124, China;* orcid.org/0000-0002-3595-6972

Sébastien Leveneur − *INSA Rouen Normandie, University of Rouen Normandie, Normandie University, LSPC UR 4704, Rouen F-76000, France;* orcid.org/0000-0001-9528-6440

Julien Legros − *Univ Rouen Normandie, INSA Rouen Normandie, CNRS, Normandie University, COBRA, Rouen F-76000, France;* orcid.org/0000-0002-4807-7897

Complete contact information is available at: https://pubs.acs.org/10.1021/acsengineeringau.5c00002

Notes

The authors declare no competing financial interest.

■ ACKNOWLEDGMENTS

This research was funded, in whole or in part, by the DFG (German Research Foundation) and the ANR (French National Research Agency) within the project MUST (MicroflUidics for Structure-reactivity relationships aided by Thermodynamics & kinetics) [ANR-20-CE92-0002-01 - Project number 446436621] and HE 7165/10-1. I.J.B. would also like to extend gratitude to ENI, the Italian national energy company, for their support and contributions. We acknowledge financial support by Technische Universität Dortmund/TU Dortmund University within the funding program Open Access Costs.

■ REFERENCES

(1) Antar, M.; et al. Biomass for a sustainable bioeconomy: An overview of world biomass production and utilization. *Renew. Sustain. Energy Rev.* **2021**, *139*, 110691.

(2) Klinksiek, M.; Baco, S.; Leveneur, S.; Legros, J.; Held, C. Activity-based models to predict kinetics of levulinic acid esterification. *ChemPhysChem* **2023**, *24* (4), No. e202200729.

(3) Bahrabadi-Jovein, I.; Seddighi, S.; Bashtani, J. Sulfur dioxide removal using hydrogen peroxide in sodium-and calcium-based absorbers. *Energy Fuels* **2017**, *31* (12), 14007−14017.

(4) Bashtani, J.; Seddighi, S.; Bahrabadi-Jovein, I. Control of nitrogen oxide formation in power generation using modified reaction kinetics and mixing. *Energy* **2018**, *145*, 567−581.

(5) Lodhi, A.; Maheria, K. C. Zeolite-catalysed esterification of biomass-derived acids into high-value esters products: Towards sustainable chemistry. *Catal. Commun.* **2024**, *187*, 106883.

(6) Mandari, V.; Devarai, S. K. Biodiesel production using homogeneous, heterogeneous, and enzyme catalysts via trans-esterification and esterification reactions: A critical review. *Bioenergy Res.* **2022**, *15* (2), 935−961.

(7) Alper, K.; et al. Sustainable energy and fuels from biomass: a review focusing on hydrothermal biomass processing. *Sustain. Energy Fuels* **2020**, *4* (9), 4390−4414.

(8) Held, C.; Sadowski, G. Thermodynamics of bioreactions. *Annu. Rev. Chem. Biomol. Eng.* **2016**, *7* (1), 395−414.

(9) Lemberg, M.; Sadowski, G. Predicting the solvent effect on esterification kinetics. *ChemPhysChem* **2017**, *18* (15), 1977−1980.

(10) Pappu, V. K.; et al. A kinetic model of the Amberlyst-15 catalyzed transesterification of methyl stearate with n-butanol. *Bioresour. Technol.* **2011**, *102* (5), 4270−4272.

(11) Patidar, P.; Mahajani, S. M. Esterification of fusel oil using reactive distillation−Part I: Reaction kinetics. *Chem. Eng. J.* **2012**, *207*, 377−387.

(12) Orjuela, A.; et al. Kinetics of mixed succinic acid/acetic acid esterification with Amberlyst 70 ion exchange resin as catalyst. *Chem. Eng. J.* **2012**, *188*, 98−107.

(13) Emel'yanenko, V. N.; et al. Renewable platform chemicals: Thermochemical study of levulinic acid esters. *Thermochim. Acta* **2018**, *659*, 213−221.

(14) Ascani, M.; Sadowski, G.; Held, C. Simultaneous Predictions of Chemical and Phase Equilibria in Systems with an Esterification Reaction Using PC-SAFT. *Molecules* **2023**, *28* (4), 1768.

(15) Riechert, O.; et al. Solvent effects on esterification equilibria. *AIChE J.* **2015**, *61* (9), 3000−3011.

(16) Baco, S.; et al. Solvent effect investigation on the acid-catalyzed esterification of levulinic acid by ethanol aided by a Linear Solvation Energy Relationship. *Chem. Eng. Sci.* **2022**, *260*, 117928.

(17) Bankole, K. S.; Aurand, G. A. Kinetic and Thermodynamic Parameters for Uncatalyzed Esterification of Carboxylic Acid. *Res. J. Appl. Sci. Eng. Technol.* **2014**, *7* (22), 4671−4684.

(18) Gross, J.; Sadowski, G. Perturbed-chain SAFT: An equation of state based on a perturbation theory for chain molecules. *Ind. Eng. Chem. Res.* **2001**, *40* (4), 1244−1260.
(19) Barker, J. A.; Henderson, D. Perturbation theory and equation of state for fluids. II. A successful theory of liquids. *J. Chem. Phys.* **1967**, *47* (11), 4714−4721.
(20) von Solms, N.; Michelsen, M. L.; Kontogeorgis, G. M. Computational and physical performance of a modified PC-SAFT equation of state for highly asymmetric and associating mixtures. *Ind. Eng. Chem. Res.* **2003**, *42* (5), 1098−1105.
(21) Gross, J.; Sadowski, G. Application of perturbation theory to a hard-chain reference fluid: an equation of state for square-well chains. *Fluid Phase Equilib.* **2000**, *168* (2), 183−199.
(22) Economou, I. G. Statistical associating fluid theory: A successful model for the calculation of thermodynamic and phase equilibrium properties of complex fluid mixtures. *Ind. Eng. Chem. Res.* **2002**, *41* (5), 953−962.
(23) Chapman, W. G.; et al. New reference equation of state for associating liquids. *Ind. Eng. Chem. Res.* **1990**, *29* (8), 1709−1721.
(24) Wolbach, J. P.; Sandler, S. I. Using molecular orbital calculations to describe the phase behavior of cross-associating mixtures. *Ind. Eng. Chem. Res.* **1998**, *37* (8), 2917−2928.
(25) Tumakaka, F.; Gross, J.; Sadowski, G. Thermodynamic modeling of complex systems using PC-SAFT. *Fluid Phase Equilib.* **2005**, *228*, 89−98.
(26) Kleiner, M.; Sadowski, G. Modeling of polar systems using PCP-SAFT: An approach to account for induced-association interactions. *J. Phys. Chem. C* **2007**, *111* (43), 15544−15553.
(27) Moine, E.; et al. I-PC-SAFT: An industrialized version of the volume-translated PC-SAFT equation of state for pure components, resulting from experience acquired all through the years on the parameterization of SAFT-type and cubic models. *Ind. Eng. Chem. Res.* **2019**, *58* (45), 20815−20827.
(28) Kleiner, M. *Thermodynamic Modeling of Complex Systems: Polar and Associating Fluids and Mixtures*; Verlag Dr. Hut, 2009.
(29) Caßens, J. *Modellierung thermodynamischer Eigenschaften pharmazeutischer Substanzen in Lösungsmitteln und Lösungsmittelgemischen*; Verlag Dr. Hut, 2013.
(30) Yaws, C. L. *Chemical Properties Handbook: Physical, Thermodynamic, Environmental, Transport, Safety, and Health Related Properties for Organic and Inorganic Chemicals*; McGraw Hill Education, 1999.
(31) Daubert, T.; Danner, R. *Data Compilation Tables of Properties of Pure Compounds*; American Institute of Chemical Engineers: New York, 1985.
(32) 10.1021/acs.iecr.5c00115.
(33) Dohrn, S.; et al. Solvent mixtures in pharmaceutical development: Maximizing the API solubility and avoiding phase separation. *Fluid Phase Equilib.* **2021**, *548*, 113200.
(34) Gmehling, J.; Onken, U.; Arlt, W. *Vapour-Liquid Equilibrium Data Collection*; Dechema, 1993.
(35) Kato, M. Vapor-liquid equilibrium measurements for binary systems of acetic acid with ethyl acetate and vinyl acetate by the dew-bubble point temperature method. *J. Chem. Eng. Data* **1988**, *33* (4), 499−501.
(36) Laube, F. S.; Sadowski, G. Predicting the extraction behavior of pharmaceuticals. *Ind. Eng. Chem. Res.* **2014**, *53* (2), 865−870.
(37) Samarov, A.; et al. Liquid−liquid equilibria for separation of alcohols from esters using deep eutectic solvents based on choline chloride: experimental study and thermodynamic modeling. *J. Chem. Eng. Data* **2019**, *64* (12), 6049−6059.
(38) Fuchs, D.; et al. Solubility of amino acids: influence of the pH value and the addition of alcoholic cosolvents on aqueous solubility. *Ind. Eng. Chem. Res.* **2006**, *45* (19), 6578−6584.
(39) Nann, A.; Held, C.; Sadowski, G. Liquid−liquid equilibria of 1-butanol/water/IL systems. *Ind. Eng. Chem. Res.* **2013**, *52* (51), 18472−18481.
(40) Laube, F.; Klein, T.; Sadowski, G. Partition coefficients of pharmaceuticals as functions of temperature and pH. *Ind. Eng. Chem. Res.* **2015**, *54* (15), 3968−3975.
(41) Pabsch, D.; et al. Influence of solvent and salt on kinetics and equilibrium of esterification reactions. *Chem. Eng. Sci.* **2022**, *263*, 118046.
(42) Veith, H.; et al. Measuring and predicting the extraction behavior of biogenic formic acid in biphasic aqueous/organic reaction mixtures. *ACS Omega* **2017**, *2* (12), 8982−8989.
(43) Altuntepe, E.; et al. Thermodynamics of enzyme-catalyzed esterifications: II. Levulinic acid esterification with short-chain alcohols. *Appl. Microbiol. Biotechnol.* **2017**, *101*, 7509−7521.
(44) Oliveira, A. C.; Moura, L. F.; Cardoso, D. Method of contribution of groups to estimate thermodynamic properties of components of biodiesel formation in liquid phase. *Fluid Phase Equilib.* **2012**, *317*, 59−64.
(45) Mekala, M.; Goli, V. R. Kinetics of esterification of methanol and acetic acid with mineral homogeneous acid catalyst. *Chin. J. Chem. Eng.* **2015**, *23* (1), 100−105.
(46) Haynes, W. M. *CRC Handbook of Chemistry and Physics*; CRC Press, 2016.
(47) Toure, O.; Dussap, C.-G. Determination of Gibbs energies of formation in aqueous solution using chemical engineering tools. *Bioresour. Technol.* **2016**, *213*, 359−368.
(48) Domalski, E. S.; Hearing, E. D. Estimation of the thermodynamic properties of C-H-N-O-S-halogen compounds at 298.15 K. *J. Phys. Chem. Ref. Data* **1993**, *22* (4), 805−1159.
(49) Chemical Properties of Methyl formate (CAS 107-31-3). 2024, https://www.chemeo.com/cid/41-465-0/Methyl-formate (accessed Sept 15, 2024).
(50) Guthrie, J. P. A group equivalents scheme for free energies of formation of organic compounds in aqueous solution. *Can. J. Chem.* **1992**, *70* (4), 1042−1054.
(51) Sahu, A.; Pandit, A. B. Kinetic study of homogeneous catalyzed esterification of a series of aliphatic acids with different alcohols. *Ind. Eng. Chem. Res.* **2019**, *58* (8), 2672−2682.
(52) Ahmedzeki, N. S.; Al-Hassani, M. H.; Al-Jendeel, H. A. Kinetic study of esterification reaction. *Al-Khwarizmi Eng. J.* **2010**, *6* (2), 33−42.
(53) Pospíšil, R.; et al. Influence of non-ideal behavior on esterification kinetics modeling. *React. Kinet. Mech. Catal.* **2020**, *130* (2), 617−632.
(54) Baco, S.; et al. Temperature effect on the steric and polar Taft substituent parameter values. *React. Chem. Eng.* **2024**, *9* (4), 833−841.

https://doi.org/10.1021/acsengineeringau.5c00002
ACS Eng. Au 2025, 5, 234−246